Lorentz lattice-gas and kinetic-walk model

Robert M. Ziff
Department of Chemical Engineering, The University of Michigan, Ann Arbor, Michigan 48109-2136

X. P. Kong and E. G. D. Cohen
The Rockefeller University, New York, New York 10021-6399

(Received 14 January 1991)

The Ruijgrok-Cohen (RC) mirror model [Phys. Lett. A **133**, 415 (1988)] of a Lorentz lattice gas, in which particles are reflected by left and right diagonally oriented mirrors randomly placed on the sites of a square lattice, is further investigated. Extensive computer simulations of individual trajectories up to 2^{24} steps in length, on a lattice of $65\,536 \times 65\,536$ sites, are carried out. This model generates particle trajectories that are related to a variety of kinetic growth and "smart" (nontrapping) walks, and provides a kinetic interpretation of them. When all sites are covered with mirrors of both orientations with equal probability, the trajectories are equivalent to smart kinetic walks that effectively generate the hulls of bond percolation clusters at criticality. For this case, 10^6 trajectories were generated, yielding with unprecedented accuracy an orbit size-distribution exponent of $\tau = 2.1423 \pm 0.0003$ and a fractal dimension of $d_f = 1.750\,47 \pm 0.000\,24$ (without correcting for finite-size effects), compared with theoretical predictions of $\frac{15}{7} = 2.142\,857\ldots$ and $\frac{7}{4}$, respectively. When the total concentration of mirrors C is less than unity, so that the trajectories can cross, the size distribution of the closed orbits does not follow a power law, but appears to be described by a logarithmic function. This function implies that all trajectories eventually close. The geometry of the trajectories does not show clear self-similar or fractal behavior in that the dependence of the mean-square displacement upon the time also appears to follow a logarithmic function. These trajectories are related to the growing self-avoiding trail (GSAT) introduced by Lyklema [J. Phys. A **18**, L617 (1985)], and the present work supports the conjecture of Bradley [Phys. Rev. A **41**, 914 (1990)] that the GSAT (the RC model with $C = \frac{2}{3}$) is not at a critical point. It is observed that when $C < 1$, the trajectories behave asymptotically like an unrestricted random walk, and so for comparison the RC model in the random walk or Boltzmann approximation (BA) is also studied. In the BA, the size distribution of returning trajectories and the geometric properties of open trajectories are investigated; the time dependence of the mean-square displacement is derived explicitly and is shown to exhibit an Ornstein-Uhlenbeck type of behavior.

I. INTRODUCTION

In this paper we consider the Ruijgrok-Cohen (RC) Lorentz lattice-gas model [1], which is defined as follows. A two-dimensional square lattice (of unit spacing) is populated with double-sided mirrors at the lattice sites (vertices). These mirrors have diagonal orientations of either $-\pi/4$ ("left") or $+\pi/4$ ("right"), and are placed randomly with probability or concentration C_L and C_R, respectively, where $C_L + C_R \leq 1$. Particles (photons) move along the bonds (edges) of the lattice at unit velocity, and undergo right-angle reflections when they encounter a mirror. Typical trajectories of a single particle are shown in Figs. 1(a) and 2(a). As can be seen in these figures, a trajectory may close on itself, forming an "orbit." Furthermore, a given bond will never be traversed for a second time in the opposite direction, as there is no way a particle can be reflected back on itself, while a bond can be traversed by a particle more than once in the same direction, but only after the trajectory has closed on itself.

This model was introduced by RC [1] as a lattice version of the Ehrenfest wind-tree model [2,3], a type of Lorentz gas in which a particle moves through a set of randomly placed, fixed scatterers in the plane. The RC model is closely related to a model proposed by Grimmett [4], a tiling model introduced by both Smith [5] and Roux and co-workers [6,7], a model of direction-rotating scatterers introduced by Gunn and Ortuño [8], and a similar model of Gates [9]. It is also closely related to a variety of kinetic-walk models and to processes that effectively generate hulls of percolation clusters [10–13] as will be discussed below. The RC model can be thought of as a kinetic lattice-gas formulation to these various kinetic-walk and tiling models.

In the RC model, the particles undergo deterministic motion in a random medium, in which the randomness (here, the position and orientation of the mirrors) is permanently frozen in. It thus differs from models where particles diffuse stochastically in a nonhomogeneous system, such as the diffusion of a particle on a percolation cluster (the "ant in the labyrinth") [14,15], or to systems that contain a permanent structure which biases the random motion of the particle [16,17]. In the RC model, the trajectory of the particle is completely determined by the fixed positions of the mirrors. Of course, the model has the stochastic component of how those mirrors are

placed and where the trajectory is started, and a meaningful characterization of this system will require an average over a large number of realizations.

The RC model (and its equivalent kinetic walks) has been investigated in a variety of situations. When the concentration of mirrors is low, the motion of the particle through the system can be approximated by a simple random walk, in which the trajectory either continues straight or randomly turns $\pm\pi/2$ (with the given probabilities), but does not "remember" what happened at that site in a future collision. In the language of kinetic theory, this is the Boltzmann approximation (BA) to the scattering problem. The fractal dimension d_f of the walk is equal to 2 as in simple Brownian motion. The dependence of the diffusion coefficient upon C_L and C_R in this approximation has been derived by Kong and Cohen [18–20]. Other kinetic-theory approximations have been investigated by Ernst, van Velzen, and Binder [21,22].

In the limit of 100% mirror coverage and symmetric orientation, i.e., $C_L = C_R = \frac{1}{2}$, the trajectories are equivalent to a growing self-avoiding trail (GSAT) [also called a kinetic growth trail (KGT)] on the Manhattan dual lattice (or the L lattice), and are isomorphic to a growing self-avoiding walk (GSAW) [also called a kinetic growth walk (KGW)] on the Manhattan lattice [12,13,23–25]. These representations are illustrated in Fig. 1. Such walks, which never get trapped, except to close at the starting position, are types of smart kinetic walks (SKW) [26] or indefinitely growing self-avoiding walks (IGSAW) [27]. The orbits have the same statistics (i.e., probability of occurence) as paths that follow the hull or perimeter (either internal or external) of a bond percolation cluster on a square lattice at criticality [4,18,25]. It follows that all trajectories (on an infinite lattice) eventually close, and that the size distribution of the orbits follows

$$P(s) \sim a_1 s^{1-\tau} \quad \text{for } s \to \infty \ , \tag{1}$$

where $P(s)$ is the probability that a trajectory closes into an orbit of s steps and a_1 is a constant, with τ given by the two-dimensional (2D) percolation hull value, $\frac{15}{7}$. Furthermore, the long trajectories are fractal with dimension $d_f = \frac{7}{4}$ [28–33]. Here the fractal dimension is defined by the asymptotic relation between the mean-square distance $\langle \Delta r^2 \rangle$ between two points on a given trajectory, and the number of steps s separating them [34]:

$$\langle \Delta r^2(s) \rangle \sim b_1 s^{2/d_f} \quad \text{for } s \to \infty \ , \tag{2}$$

where b_1 is a constant, and the brackets indicate an average over many pairs of points on one or more trajectories whose size (total number of steps) is much greater than s. Thus, the motion of a test particle on open trajectories obeys a kind of enhanced diffusion, because the mean-square displacement grows faster than the time ($\sim s^{8/7}$). On the other hand, if one averages over orbits of all sizes including small ones, or equivalently puts particles randomly throughout the system without selecting the large or "incipient" percolating orbits only, then the average mean-square displacement of all particles $\langle \Delta r^2(s) \rangle$ becomes proportional to s as in classical diffusion, where the bar indicates an average over all possible starting points on the lattice. This diffusion, however, is anomalous in that the probability distribution is not Gaussian [28].

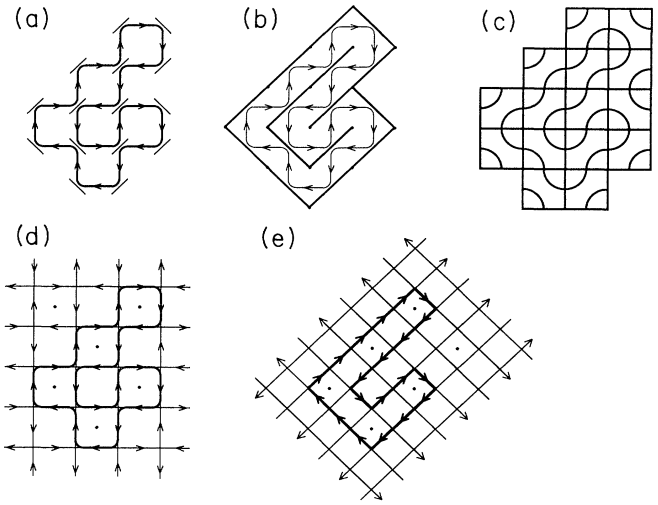

FIG. 1. (a) A typical orbit of the RC model when $C_L + C_R = 1$. In (b), the mirrors are represented as bonds on the percolation lattice (inner bonds) and its dual (outer bonds), while in (c) they are represented as two different orientations of tiles [5–7]. In (d), the trajectory is also represented as a growing self-avoiding trail (GSAT) on a Manhattan covering lattice, in which the allowed directions of the "streets" alternate at every block. In a GSAT, the particle can revisit a site but cannot traverse a bond more than once. In (e), the walk is shown as a growing self-avoiding walk (GSAW) on the Manhattan lattice. In this walk, the particle must follow the allowed directions of the Manhattan lattice and cannot visit a site more than once. In both (d) and (e), when there are two ways that the particle can continue, the particle chooses each with equal probability when $C_L = \frac{1}{2}$. The underlying percolation lattice is shown by dots. The net effect of these two walks is to generate paths around random percolation cluster [12,13]. In all representations, there are 15 steps or places where one of two possible choices must be made.

When $C_L + C_R < 1$, the trajectories are no longer isomorphic to percolation cluster hulls in an obvious way. In this case, Kong and Cohen [18] have found (by computer simulation) that $\langle \Delta r^2 \rangle \sim 4Ds$ still holds, with the diffusion coefficient D dependent upon the concentration of the mirrors. However, many questions remain: Do all these trajectories ultimately close into orbits when $C_L + C_R < 1$? Are the individual trajectories fractal? What is the nature of the size distribution of the orbits?

To begin to answer these questions, we have carried out extensive computer simulations of the RC model for various values of the mirror concentration. In contrast to the work in Ref. [18], here we consider only individual trajectories. These trajectories were generated on a blank (undetermined) lattice by a kinetic growth algorithm in which the probability of the particle continuing straight is $1 - C_L - C_R$, and of making a turn is C_L or C_R. Once a

site has been visited, a mirror (or straight marker) is placed there for the duration of the given trajectory. It can be seen that this process generates trajectories with the same probability as they would be found in a system already populated with mirrors, as considered in Ref. [18]. We also made use of a programming technique [10] that allows the simulation of growth processes on very large virtual lattices (here $65\,536\times65\,536$) using a moderate size computer (Apollo DN 4000, with 8 Mbyte of random-access memory). With a lattice this large, we were able to generate open and closed trajectories of up to $2^{24}=16\,777\,216$ steps without the trajectories approaching the system boundary. Thus, we were able to get statistics unbiased by boundary effects, and subject only to a finite-size cutoff of a very large value. More details of the simulation method, as well as the data analysis, are given in Sec. II.

We considered only the symmetric case where $C_L=C_R\equiv C/2$. First of all, we carried out a new study of the case $C=1$, in which case the trajectory is a SKW that generates the hull of a bond percolation cluster, as shown in Fig. 1. This model serves as a comparison for the other cases, as well as a check of our programming and analytical techniques. A previous study of percolation hulls by one of us [31] considered site rather than bond percolation. Grassberger [11] has carried out a simulation of bond percolation hulls; however, it was of a somewhat different nature and does not provide the information we are interested in. Here we have simulated 10^6 trajectories, using a cutoff of $2^{21}=2\,097\,152$ steps, in contrast to the 30 000 trajectories with cutoff of $2^{20}=1\,048\,576$ that were used in Ref. [31], for example. The present work represents the results of a significant amount of computer time (many months) as a total of well over 10^{11} particle steps were simulated. This work yields $\tau=2.1423\pm0.0003$ for the size distribution exponent, which is consistent with the theoretical value of $\frac{15}{7}=2.142\,857\ldots$, and $d_f=1.750\,47\pm0.000\,24$ for the fractal dimension, consistent with the theoretical value [30,32] of $\frac{7}{4}$. The slightly high value of d_f can be attributed to a "finite-size" effect of the size cutoff, which produces a measurable decrease in $\langle\Delta r^2\rangle$ down to separation of less than 2^{16} steps. The details of the work for $C=1$ are given in Sec. III.

When $C<1$, some of the sites have no mirrors where the particle trajectories cross, as shown in Fig. 2. In this figure, we also show the correspondence of the RC model to a generalized tiling model [5–7]; besides the left and right tiles, one must add "crossing" tiles for the straight segments. When $C<1$, we find that the trajectories are not simply fractal. For very long times, the mean-square displacement appears to approach a linear function of time multiplied by a logarithmic function, which implies that the trajectories are not self-similar (fractal). Secondly, we find that the size distribution of closed orbits also is *not* described by a power law, but again appears to show logarithmic behavior. This logarithmic function implies that all trajectories eventually close.

The trajectories for the RC model are essentially growing self-avoiding trails [35] (GSAT). A self-avoiding trail (SAT) is a path that can cross itself at lattice sites, but

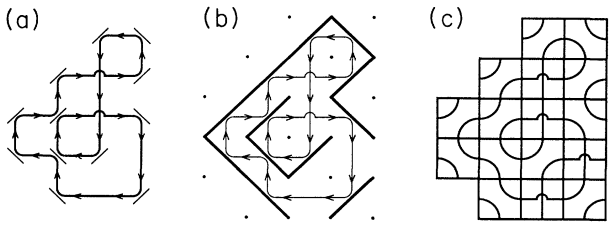

FIG. 2. (a) An example of the RC model with $C<1$. Now there are sites with no mirrors, where trajectories will cross. (b) The representation showing the mirrors as percolation bonds on the underlying lattice and its dual lattice. (c) The equivalent tiling representation, where new "crossing tiles" (where the trajectory crosses) must be put at the site corresponding to no mirror.

cannot traverse a given bond more than once [25], and a *growing* SAT is one that is produced in a step-by-step fashion. It can be seen that in the growth algorithm that we use to generate trajectories for the RC model, the mirrors (which are placed the first time a site is visited) guarantee that when that site is revisited, the trajectory will always turn to avoid recrossing previously traversed bonds, except after returning to the origin. When $C=\frac{2}{3}$, the RC model corresponds precisely to the standard GSAT introduced by Lyklema [35], in which the walker steps with equal probability ($\frac{1}{3}$) in each of the three allowed directions—forward, right, or left—after visiting a blank site. Lyklema believed the resulting walks to be fractal with $2/d_f=1.070\pm0.006$, based upon trails of 2000 steps. While our data agree with Lyklema's for trajectories up to that size, they do not bear out his extrapolation for larger trajectories. Rather, our conclusions about the GSAT agree with a recent prediction of Bradley [23], who showed that the GSAT obtains for a self-attracting SAT at a temperature that is somewhat outside the transition temperature found by Meirovitch and Lim [36]. (A self-attracting SAT is a model for a polymer chain in which there is a short-ranged intermolecular potential between the particles along the chain.) From this result, Bradley concludes that the GSAT is not at a critical point, implying that d_f should approach 2 for long walks, and the size distribution should not show a power-law behavior—as we have observed. The results for $C<1$ are presented in Sec. IV.

The simulations of the particles when $C<1$ suggests that over large length scales, the trajectories act (in some sense) like an unrestricted random walk. To investigate that analogy, we have also considered the RC model in the Boltzmann approximation (RC-BA), for the case of $C=1$. Here $P(s)$ is the first-passage return probability in s steps, and is analogous to the orbit-size distribution in the RC model. $P(s)$ can be found exactly by means of a recursion relation, and does not satisfy (1) but instead is described by a logarithmic function. In fact, we show that a logarithmic function of the same form describes the $P(s)$ of the RC model when $C<1$. We also carried out computer simulations of the RC-BA model to study the geometrical properties of the trajectories. While the

random-walk nature of this model implies (2) should be obeyed with $d_f=2$ for large s, we find that the (necessary) use of a cutoff (at $s^*=2^{21}$) again leads to measurable effects on the behavior of the mean-square displacement at large separations.

We have not considered cases where $C_L \neq C_R$, but leave this for future work. We have calculated the complete time dependence of the mean-square displacement for general C_L and C_R in the RC-BA model, and find that this model represents an Ornstein-Uhlenbeck process [37]. In the limit of large times, the mean-square displacement is linear in the time with a diffusion coefficient in agreement with previous work [18–20]. These results are presented in an appendix. Finally, the conclusions and suggestions for further work are presented in Sec. VI.

II. SIMULATION PROCEDURE

A. The trajectory-generating algorithm

Individual trajectories were generated by a trajectory growth algorithm, in which the lattice starts out completely blank (undetermined), and mirrors are placed at lattice sites as they are visited by the particle. The four directions are labeled 0, 1, 2, and 3 in counterclockwise order. The effect of a right mirror is to change a direction d into $(1-d)$ mod 4, while the effect of a left mirror is to change d into $3-d$. (We note that, in contrast, in the Gunn-Ortuño [8] model, a clockwise-rotating scatterer changes d into $(d-1)$ mod 4 and a counterclockwise rotating scatterer changes d into $(d+1)$ mod 4. These two models can be shown to be equivalent only when $C_L=C_R=\frac{1}{2}$.)

The particle is started at the origin of the blank lattice, with unit velocity in an arbitrary direction (say 0). It then moves to the nearest neighbor [coordinates (1,0)], where a left or right mirror is placed with the appropriate probability, changing the direction of the particle accordingly. When $C_L+C_R<1$, there is also a possibility that no mirror is placed at the site, and the particle continues straight. The state of each site (left mirror, right mirror, or no mirror) is fixed for the duration of the simulation of each individual particle's trajectory in the (not unlikely) event that the site is revisited by the particle. The procedure is repeated until the particle is back at the origin with a velocity in the direction 0, or until the upper size cutoff is reached.

Although we only put down mirrors as we go along, the statistics are clearly the same as if the mirrors existed previously, since the mirrors are placed with independent probability, and once determined, are not changed for the duration of each particular trajectory.

B. Data analysis procedure

The *size* of a trajectory s is defined as the length of the trajectory or the number of steps along the lattice bonds. It is thus equivalent to the time elapsed, since the velocity is assumed to be unity. The statistics of s were analyzed by making a histogram, as follows. If a trajectory has closed on itself before the cutoff was reached, the occupation number of a bin representing the size of the trajectory was increased by 1. We used base-2 logarithmic bins representing orbit sizes in the range of 4–7, 8–15, 16–31, ... steps (index 2, 3, ...). That is, the occupation number of the bin B_n' is equal to the number of orbits whose size s is in the range $2^n \le s < 2^{n+1}$. The normalized occupation is given by $B_n=B_n'/N$, where N is the total number of trajectories simulated (i.e., realizations). Thus B_n is the probability that the size falls in the nth bin, and is related to $P(s)$ by

$$B_n=\sum_{s=2^n}^{2^{n+1}-1} P(s) \ . \tag{3}$$

The value of B_{n^*}' at the cutoff $n=n^*=\log_2(s^*)$ is equal to the number of trajectories that have just closed, or are still open, when s reaches s^*. The normalized value $B_{n^*}=B_{n^*}'/N$ is related to $P(s)$ by

$$B_{n^*}=\sum_{s=2^{n^*}}^{\infty} P(s) \ . \tag{4}$$

In the simulations presented here, we used cutoffs of $n^*=21$ and 24, resulting in 20 or 23 values of B_n (as $B_0=B_1=0$).

We define $N(s)$ as the probability that a trajectory closes in s, or greater, steps:

$$N(s)=\sum_{s'=s}^{\infty} P(s') \ . \tag{5}$$

When $s=2^n$, for $n=2, 3, \ldots$, we write $N_n=N(2^n)$. This quantity can be found from the B_n by

$$N_n=\sum_{n'=n}^{n^*} B_{n'} \ , \tag{6}$$

and $N_{n^*}=B_{n^*}$.

If the size distribution (1) holds, then it follows that

$$N(s) \sim a_2 s^{2-\tau} \quad \text{for } s \to \infty \ , \tag{7}$$

where $a_2=a_1/(\tau-2)$. To determine τ from N_n, we introduce the following quantity:

$$\begin{aligned} X_n &= \log_2(N_n/N_{n+1}) \\ &= \log_2(1+B_n/N_{n+1}) \ . \end{aligned} \tag{8}$$

If $N(s)$ obeys (7), then $X_n \to \tau-2$ as $n \to \infty$. However, the converse of this statement is not necessarily true: if $X_n \to$ const, it does not necessarily follow that $N(s) \sim s^{-\tau}$, since $N(s)$ may also contain logarithmic terms. The latter would be seen by a very slow approach of X_n to a constant value. In fact, we will find this behavior occurs in some cases below.

Note X_n is the slope of the line connecting the two points at n and $n+1$ on a plot of $\log N_n$ versus n, and is consequently a sensitive characterization of the size distribution behavior. However, X_n is susceptible to numerical fluctuations and thus requires quite precise data [compared with a simple log-log plot of $N(s)$ versus s].

When (7) is applicable (i.e., the case $C=1$), we will also consider a "running average" of the values of X_n, starting

from the maximum, defined as follows: $\bar{X}_{n^*-1}=X_{n^*-1}$, $\bar{X}_{n^*-2}=(X_{n^*-1}+X_{n^*-2})/2$, or in general

$$\bar{X}_n \equiv \frac{1}{n^*-n}\sum_{n'=n}^{n^*-1} X_n = \frac{1}{n^*-n}\log_2\left[\frac{N_n}{N_{n^*}}\right] . \tag{9}$$

Thus $\bar{X}_n$ is the slope of the line connecting the points at n and n^*, on a plot of $\log_2 N_n$ versus n. It follows that $\bar{X}_n$ also tends to $\tau-2$ for large n if $N(s)$ follows (7); however, this quantity has smaller fluctuations than the X_n because of the larger difference between the numerator and denominator in the logarithmic function in (9).

The trajectories that remained open at the cutoff were used to study the geometric or fractal properties. For these trajectories, we created a list of the x and y coordinates of every point 64 steps apart. For a cutoff of $s^*=2^{21}$, this list contained $2^{15}+1=32\,769$ entries (including the coordinates of the starting point). The list was analyzed as follows. First the square distances between each of the 32 768 adjacent entries on the list were averaged, yielding the mean-square distance of points separated by 64 steps on the trajectory, $\langle \Delta r^2(64)\rangle$. Then the distances between the 32 767 pairs of coordinates two apart on the list were averaged, yielding $\langle \Delta r^2(128)\rangle$, the distances between the $32\,769-4=32\,765$ pairs of coordinates four apart on the list, yielding $\langle \Delta r^2(256)\rangle$, and so on. Note that while the final value $\langle \Delta r^2(2^{21})\rangle$ made use of only a single measurement between the first and last points on the list, the penultimate value $\langle \Delta r^2(2^{20})\rangle$ made use of distances between 16 385 pairs of points. For $128 \le s \le 2^{20}$ we thus used overlapping pairs of points from the list. In total, 458 769 distance measurements were used from each trajectory, resulting in 16 values of $\langle \Delta r^2(s)\rangle$, for points separated by $s=2^6, 2^7, \ldots, 2^{21}$ steps. Likewise, for a cutoff of 2^{24} the list for each trajectory contained 262 145 entries, from which 4 458 868 square distance measurements were made, and yielded 19 values of $\langle \Delta r^2(s)\rangle$.

To analyze these measurements of $\langle \Delta r^2(s)\rangle$, we introduce the quantity

$$Y(s) \equiv \log_2[\langle \Delta r^2(2s)\rangle / \langle \Delta r^2(s)\rangle] , \tag{10}$$

which is the slope of the line connecting the points at s and $2s$ on a plot of $\log\langle \Delta r^2(s)\rangle$ versus $\log s$. If Eq. (2) is valid, then $Y(s)\to 2/d_f$ as $s\to\infty$. Note that the limiting behavior of X and Y that follows from (1) and (2) differs by exactly unity if the hyperscaling relation $2/d_f=\tau-1$ is valid. We also introduce the notation $Y_n \equiv Y(2^n)$ and $\langle \Delta r_n^2\rangle \equiv \langle \Delta r^2(2^n)\rangle$, and write (10) as

$$Y_n = \log_2[\langle \Delta r_{n+1}^2\rangle / \langle \Delta r_n^2\rangle] . \tag{11}$$

C. Image storage

The image storage (compression) scheme introduced in Ref. [8] was implemented here as follows: a virtual lattice of $65\,536\times 65\,536$ sites was used. This lattice was conceptually divided into 256×256 blocks of 256×256 sites each. Of the 16 bits of the x and y coordinates of each lattice point, the upper 8 bits were used to determine the block in which the point falls, while the lower 8 bits determine the point's position within that block. Actual memory was not assigned to a block until the particle entered it. In order to keep track of the memory assignments, a 256×256 array was used as a "lookup table" to tell where in the memory that block was assigned. This array gives the upper part or the so-called "offset" of the actual memory address, while the lower part of the address comes from the lower 8 bits of the x and y coordinates. Actually, only one-dimensional arrays were used, and the application of bit shifting, masking, etc., made the whole process very fast and efficient—nearly the same speed as a typical lookup in a standard two-dimensional array.

The advantage of this scheme is that only a small fraction of the memory for a $65\,536\times 65\,536$ array is actually used. Allowing two bits for each lattice point for the four states—blank (unspecified), left mirror, right mirror, and no mirror—this array would require $4\times 65\,536^2/8 = 2^{31}\approx 2\times 10^9$ bytes of fast memory (one byte = 8 binary places), which is available on only the largest existing computers. However, when a typical simulation of the RC model is carried out, only a small region of the lattice is actually visited. This is partly because the trajectory is ramified, but also simply because there is a tendency for the trajectory to go off far in just one direction from the origin and never visit other parts of the lattice. By using our storage scheme, we do not have to reserve memory for these areas that are never visited.

Another advantage of this memory allocation procedure comes in resetting the lattice to the blank condition, which must be done after each trajectory is completed. For a large array, this operation itself would take a significant amount of time, and would be required for each trajectory, even very small closed ones. In our method, only the blocks that have been entered by the trajectory need to be reset when the trajectory is complete, significantly reducing the average time required for this operation.

Typically, slightly more than one byte of memory in the main data array was used for each step of a trajectory, for long trajectories. For example, for the simulations of trajectories that reached the cutoff of $2^{21}=2\,097\,152$ steps at $C=1$, about 2.4 Mbyte of memory were used (about one-thousandth of the memory that would be required for the entire lattice). Since a byte stores four data points, this memory can store about 10^7 points. Thus, about 20% of the allocated memory was assigned to occupied sites—a fairly high percentage. An additional array of 65 536 32-bit integers was used for the block lookup table. The latter can be thought of as the memory "overhead" for this procedure, and can be seen to be relatively small.

III. RESULTS FOR $C=1$

A. Orbit-size distribution

For $C=1$ we generated a total of 10^6 trial trajectories, using a cutoff of $s^*=2^{21}$ steps. Here we carry a detailed analysis of the data and its errors. We note that these data may be useful for future studies of finite-size corrections.

TABLE I. Statistics from the simulation of 10^6 trajectories of the RC model with $C=1$. B_n ($n<21$) is the fraction of orbits whose size (total length) was in the interval $(2^n, 2^{n+1}-1)$, while B_{21} is the fraction of trajectories that did not close at the cutoff $n^*=21$. N_n is the upper cumulative distribution, and X_n and $\bar{X}_n$ are estimates of $\tau-2$, as explained under Eqs. (8) and (9). The numbers in parentheses represent the errors in the last digit(s).

n	B_n	N_n	X_n	$\bar{X}_n$
2	0.125 46(37)	1.000 00	0.1934(6)	0.1485(2)
3	0.099 30(34)	0.874 54(37)	0.1739(6)	0.1460(2)
4	0.080 13(28)	0.775 24(40)	0.1574(6)	0.1444(2)
5	0.068 87(24)	0.695 11(42)	0.1505(6)	0.1436(2)
6	0.060 48(22)	0.626 24(50)	0.1465(5)	0.1431(2)
7	0.054 10(22)	0.565 76(51)	0.1450(6)	0.1429(2)
8	0.048 74(23)	0.511 67(51)	0.1444(7)	0.1427(2)
9	0.043 81(20)	0.462 93(53)	0.1434(6)	0.1426(3)
10	0.039 88(18)	0.419 12(47)	0.1443(7)	0.1425(3)
11	0.035 87(19)	0.379 23(49)	0.1433(8)	0.1423(3)
12	0.032 00(14)	0.343 36(50)	0.1412(6)	0.1422(3)
13	0.029 28(20)	0.311 36(48)	0.1425(9)	0.1423(4)
14	0.026 51(18)	0.282 08(42)	0.1424(10)	0.1423(4)
15	0.023 97(17)	0.255 58(43)	0.1421(10)	0.1423(5)
16	0.021 56(16)	0.231 60(40)	0.1410(10)	0.1423(5)
17	0.019 68(14)	0.210 04(36)	0.1419(10)	0.1426(6)
18	0.017 86(14)	0.190 36(35)	0.1421(11)	0.1429(7)
19	0.016 35(13)	0.172 50(34)	0.1437(12)	0.1433(8)
20	0.014 72(10)	0.156 15(33)	0.1428(11)	0.1428(11)
21	0.141 43(34)	0.141 43(34)		
Total	1.000 00			

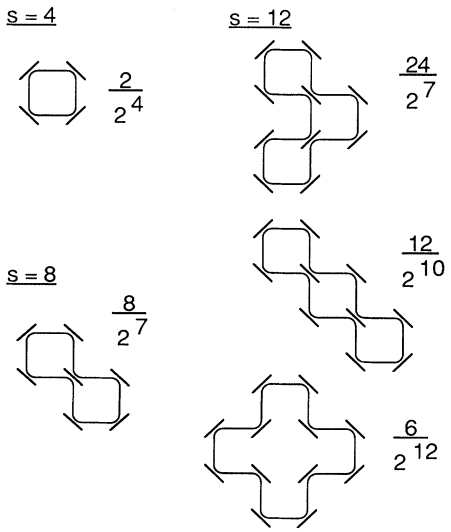

FIG. 3. Probability of generating orbits of less than $s=16$ steps in length, for the RC model with $C=1$. In each weight, the power of 2 in the denominator reflects the probability that the mirrors occur in the given orientation (probability $\frac{1}{2}$ for each mirror), and the numerator gives the number of distinct ways the given orbit (including rotated and reflected versions) can be generated.

In Table I we list the data on the orbit-size distribution. The errors listed in this table were calculated as follows: Of the 95 separate computer runs, 66 were of exactly 10 000 trajectories each. For these 66 runs, we calculated the standard deviation of each quanity then divided by $\sqrt{66}$ to find the expected error. This error was then extrapolated to the total of 10^6 trajectories by multiplying it by $(6.6\times10^5/10^6)^{1/2}$. In other words, we used the full 10^6 trajectories to find the mean values, and the 6.6×10^5 trajectories in the uniform runs to estimate the errors in the mean.

The first entry gives the fraction of trajectories in each bin, B_n. We can check the first two entries of B_n using an exact enumeration of the possible orbits, which is shown in Fig. 3. The only contribution to B_2 is from a simple square orbit ($s=4$), which occurs with probability $\frac{1}{8}$, and the entry in Table I gives $B_2=0.125\,46\pm0.000\,37$. Likewise, for B_3 we get probability $\frac{1}{16}$ for the trajectories of size 8, plus $\frac{3}{128}+\frac{3}{256}+\frac{3}{2048}$ for trajectories of size 12, for a total expected number $\frac{203}{2048}=0.099\,12$, compared with a measured value $B_3=0.099\,30\pm0.000\,34$. Thus the measured values and error bars prove to be consistent with the exact results.

Next in Table I we list the cumulative distribution function N_n and the quantities X_n and $\bar{X}_n$ calculated from (8) and (9). These values of X_n and $\bar{X}_n$ are plotted in Fig. 4. It can be seen that the X_n approach a constant for $n\gtrsim11$, whose value is consistent with the theoretical prediction [10,31,32] $\tau-2=\frac{1}{7}=0.142\,857\ldots$ within about ±0.001. Because X_n approaches a constant—implying

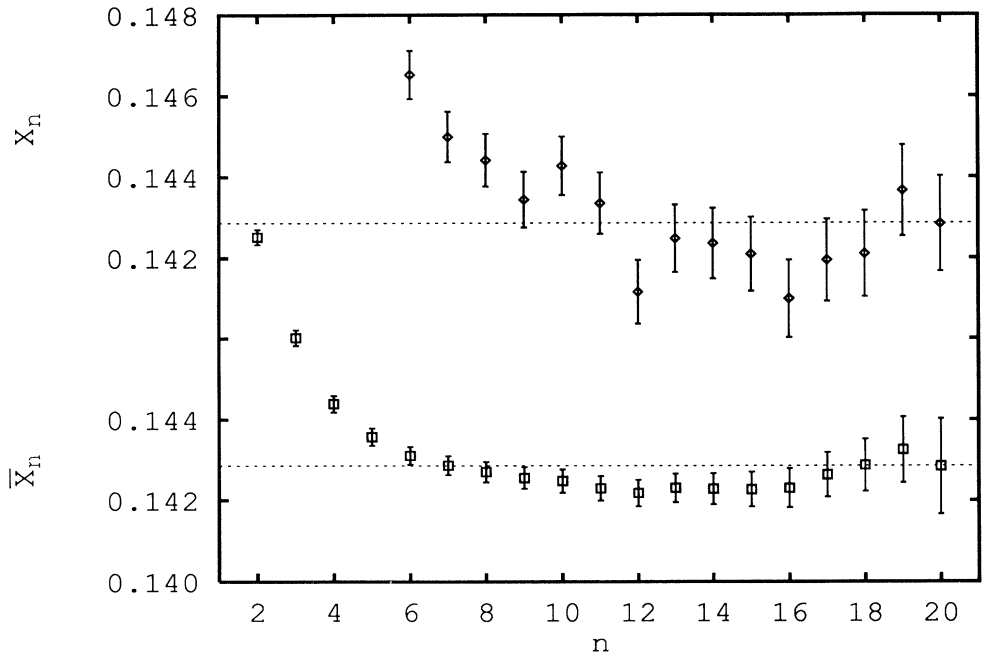

FIG. 4. The values of X_n ($\Diamond$) and $\bar{X}_n$ ($\Box$) for the RC model with $C=1$, plotted as a function of $n=\log_2(s)$. X_n is the slope of the line connecting two adjacent data points of N_n-n on a log-log plot, while $\bar{X}_n$ is the slope between the point at n and the point at the cutoff. It can be seen that finite-size effects in $\bar{X}_n$ become insignificant for $n \gtrsim 11$. The theoretical asymptotic value $\frac{1}{7}$ (— — —) is shown for comparison.

that (1) is followed—it is appropriate to consider the average $\bar{X}_n$. It can be seen in Fig. 4 that $\bar{X}_n$ also approaches $\frac{1}{7}$, and that the finite-size effects (apparent only for $n \lesssim 10$) and fluctuations are smaller than those for X_n. Taking $\bar{X}_{11}$ as the most precise value of $\bar{X}_n$ still unbiased by the finite-size effects, we obtain $\tau-2=0.1423\pm0.0003$. The theoretical value is within two error bars (standard deviations) of this result. Note that in this determination of τ, we did not need to consider finite-size corrections, which generally necessitates the simultaneous use of other critical exponents. Our error in τ is just 0.014%.

As mentioned above, the errors in each of the quantities in Table I were determined by analyzing their fluctuations in 66 separate runs. In fact, these errors can also be predicted theoretically, since the data represent the results of independently sampling a given distribution (which, of course, we are trying to determine). If a certain event "1" (such as an orbit size falling in a certain bin) occurs with probability p, then after N trials, the expected number of occurrences of "1" (divided by N), and its standard deviation will be given by

$$\mathcal{E}(n_1/N)=p\pm[p(1-p)/N]^{1/2}\,, \tag{12}$$

where the value of p can be estimated from the observed number of occurrences, that is, from n_1/N. Equation (12) can be derived from a straightforward application of probability theory. It can be used to estimate the errors in B_n and N_n. For example, for B_4, Table I gives $B_4=0.080\,13=p$, and (12) predicts an expected error of $\pm0.000\,27$, compared with the measured error of $\pm0.000\,28$ (Table I). In a similar way, one can verify that all the observed errors in the B_n and N_n are consistent with (12).

To determine the errors in X_n and $\bar{X}_n$, we need to know the statistical properties of ratios of occurrences of two different events (such as, those of an orbit size falling in two different bins). Let "1" and "2" be two disjoint events, occurring with probabilities p and q, respectively, where $p+q\leq 1$—equality occurring when there are no other possible outcomes. Let n_1 and n_2 be the number of occurrences of these two events. By being disjoint, we mean that there are no common elements, or, in other words, that no single event increments both n_1 and n_2. We find that the expected value and the standard deviation of the ratio of n_1/n_2 in a sample of N trials (asymptotically for large N) are given by

$$\mathcal{E}(n_1/n_2)=\frac{p}{q}\pm\left[\frac{p(p+q)}{q^3N}\right]^{1/2} \tag{13}$$

for large N. In order to use (13) to estimate the error in X_n, one must use the second formula in (8) for X_n, because it involves the ratio of B_n and N_{n+1}, which are disjoint quantities. [The first formula in (8) cannot be used because N_n and N_{n+1} are not disjoint—there are events that increase both of these quantities.] Then, using $p=B_n$ and $q=N_{n+1}$, (13) gives the error in B_n/N_{n+1}, and then from (8) we find that X_n will have an estimated

error of

$$\pm\frac{1}{\ln 2}\left[\frac{1}{N}\left[\frac{1}{N_{n+1}}-\frac{1}{N_n}\right]\right]^{1/2}. \quad (14)$$

For example, for the error in X_4, using $N_5=0.595\,00$ and $N_4=0.775\,24$, we find ± 0.0006, which agrees with the measured error (Table I).

In the calculation of the errors of $\bar{X}_n$, it is necessary to rewrite the ratio N_n/N_{n*} in (9) as $1+(N_n-N_{n*})/N_{n*}$, since N_n-N_{n*} and N_{n*} are disjoint quantities. Then (13) can be applied to find the expected error of this ratio, and from (9) we find that the error in $\bar{X}_n$ is given by

$$\pm\frac{1}{(n^*-n)\ln 2}\left[\frac{1}{N}\left[\frac{1}{N_{n*}}-\frac{1}{N_n}\right]\right]^{1/2}. \quad (15)$$

The predictions of this formula agree with the observed errors in the $\bar{X}_n$. In the following simulations, we will use the above formulas to estimate the errors in these quantities.

B. Geometric properties

In Table II we list $\log_2\langle\Delta r_n^2\rangle$ and the slope between successive points Y_n determined from the 141 433 trials (out of 10^6) that remained open at the cutoff, $n^*=21$. The values of Y_n are plotted in Fig. 5 and show that besides the typical finite-size effects for small length scales (here, $n\lesssim 13$), there is another "finite-size" effect that causes the slope Y_n to decrease again for $n\gtrsim 15$. Presumably, this decrease occurs because many of the open trajectories that were used to find Y_n were in fact close to closing when the cutoff was reached and consequently were more compact on large length scales than a corresponding piece of an infinite walk would be. We have ob-

TABLE II. The geometric properties of 141 433 trajectories still open at 2^{21} steps, out of 10^6 realizations, for the RC model with $C=1$. $\langle\Delta r_n^2\rangle$ is the mean-square distance between pairs of points separated by 2^n steps along those trajectories. The quantity Y_n, defined in Eq. (11), is an estimate for $2/d_f=\frac{8}{7}=1.142\,857\ldots$. The finite-size effects are evidently smallest for $n\approx 14$, since Y_n reaches its maximum value there. The Y_n are plotted in Fig. 5.

n	$\log_2\langle\Delta r_n^2\rangle$	Y_n
6	6.6139(0)	1.133 03(1)
7	7.7469(0)	1.137 24(1)
8	8.8842(0)	1.139 73(2)
9	10.0239(0)	1.141 15(2)
10	11.1650(0)	1.141 95(3)
11	12.3070(1)	1.142 39(5)
12	13.4494(1)	1.142 53(7)
13	14.5919(1)	1.142 48(10)
14	15.7344(2)	1.142 55(15)
15	16.8769(2)	1.142 19(22)
16	18.0191(4)	1.141 53(36)
17	19.1606(6)	1.141 44(48)
18	20.3021(8)	1.138 84(84)
19	21.4409(11)	1.120 98(137)
20	22.5619(20)	1.051 90(237)
21	23.6138(30)	

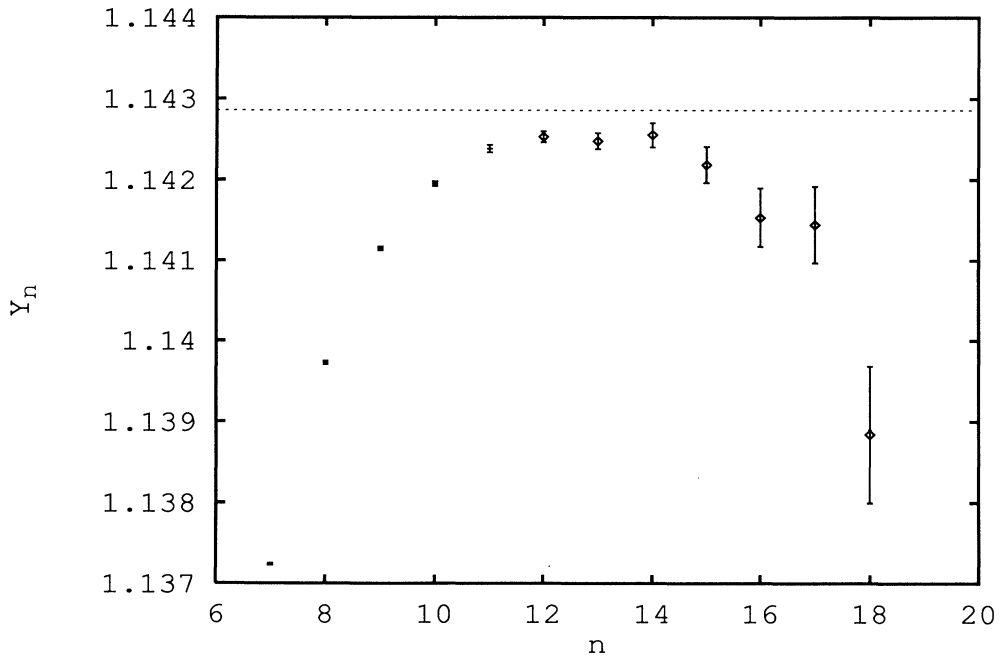

FIG. 5. The values of Y_n for the RC model with $C=1$ taken from Table II, plotted as a function of n. For small n there are finite-size effects due to the lattice spacing, and for large n there are finite-size effects caused by the cutoff at $n^*=21$. The theoretical asymptotic value $\frac{8}{7}$ (— — —) is shown for comparison.

served this effect for separations as small as 2^{15} steps, which is $\frac{1}{32}$ the total length of these trajectories. Note, however, that the y axis in Fig. 5 has a highly expanded scale, and a peak is only evident because of our precise data. No matter how large a size cutoff is used, a peak in Y_n will always be seen with sufficiently precise data, because of the two finite-size effects.

The errors here were estimated from analyzing the runs of 10 000 trials each. We cannot estimate these errors from a formula like (12) or (13), because the measurements of $\langle \Delta r_n^2 \rangle$ are not independent random quantities.

We take the maximum value $Y_{15}=1.142\,55\pm0.000\,15$ as the best estimate for $2/d_f$. This implies $d_f=1.750\,47\pm0.000\,24$, which is slightly greater than the theoretical value of $d_f=\frac{7}{4}$. We have not made any corrections for the two finite-size effects, which may explain the small discrepancy in d_f (which, however, is still within two standard deviations of the exact value). The values of $\langle \Delta r^2 \rangle$ near this peak imply that $b_1 \approx 0.8315$, where b_1 is defined in (2).

IV. RESULTS FOR $C < 1$

A. Orbit-size distribution

We carried out simulations for $C=\frac{2}{3}$, 0.8, 0.98, and 0.998 with $n^*=21$, using 30 000–150 000 trajectories each. The measured values of B_n are listed in Table III. As C decreases, the number of open trajectories at the cutoff, B_{21^*}, rapidly increases. Because the trajectories that reach the cutoff require the most time to generate, and furthermore are used to calculate the mean-square distances, which is quite time consuming, the amount of computational work for a given number of trajectories increased rapidly for smaller C.

The value of B_2, which gives the probability of the orbit closing in 4–7 steps, decreases as C decreases. An exact enumeration similar to that shown in Fig. 3 but for $C<1$ yields $B_2=(C^4/8)[1+3(1-C)^2]$, or $B_2=0.0329$, 0.0573, 0.1154, and 0.1240 for $C=\frac{2}{3}$, 0.8, 0.98, and 0.998, respectively. In comparison, the measured values from Table III and the errors bars calculated from (13) are 0.0325 ± 0.0005, 0.0561 ± 0.0012, 0.1169 ± 0.0016, and 0.1225 ± 0.0019, respectively. Thus, these results are consistent with the exact results.

Figure 6 shows the plot of X_n for the four values of $C<1$, along with the plot for $C=1$. The deviations from the behavior for $C=1$ are striking. Even for $C=0.998$, X_n follows the behavior of $C=1$ only to about $n=8$, and then begins to decrease markedly, in spite of the fact that after 512 steps ($n=9$) the expected number of straight segments is only $(0.002)(512)\approx 1$. The values of X_n keep dropping and do not reach a constant value, so that even at 2^{21} steps, the size distribution is not consistent with a power law. For smaller values of C, a more pronounced decrease in X_n is seen, and there are observable differences with $C=1$ already when $n=2$. The curve for

TABLE III. The first four columns give B_n of the RC model for $C<1$. The actual number of trajectories N simulated for each value of C is shown in parentheses. The last column gives B_n for the RCBA model (with $C=1$), determined recursively from (25) and (26); the exact enumeration of B_2 and B_3 for this model is illustrated in Fig. 11. The resulting X_n and $1/N_n$ (for both models) are plotted in Figs. 6 and 7, respectively.

n	$C=\frac{2}{3}$ (150 000)	$C=0.8$ (36 000)	$C=0.98$ (40 500)	$C=0.998$ (30 000)	$c=1.0$ (BA) (exact)
2	0.0325	0.0561	0.1169	0.1225	0.125 000 000
3	0.0284	0.0444	0.0900	0.0980	0.087 890 625
4	0.0268	0.0380	0.0709	0.0795	0.066 834 867
5	0.0239	0.0326	0.0576	0.0691	0.054 195 228
6	0.0234	0.0283	0.0502	0.0612	0.045 713 557
7	0.0216	0.0271	0.0427	0.0531	0.039 487 992
8	0.0205	0.0244	0.0365	0.0482	0.034 635 229
9	0.0189	0.0226	0.0329	0.0420	0.030 703 967
10	0.0186	0.0225	0.0277	0.0369	0.027 438 784
11	0.0179	0.0203	0.0244	0.0334	0.024 680 704
12	0.0168	0.0188	0.0226	0.0274	0.022 322 534
13	0.0159	0.0178	0.0188	0.0239	0.020 287 393
14	0.0150	0.0169	0.0187	0.0223	0.018 517 617
15	0.0150	0.0164	0.0165	0.0194	0.016 968 575
16	0.0141	0.0159	0.0144	0.0176	0.015 604 949
17	0.0140	0.0144	0.0132	0.0137	0.014 398 334
18	0.0132	0.0131	0.0121	0.0134	0.013 325 610
19	0.0121	0.0132	0.0113	0.0111	0.012 367 767
20	0.0117	0.0131	0.0101	0.0095	0.011 509 050
21	0.6400	0.5441	0.3124	0.1979	0.318 117 219
Total	1.0000	1.0000	1.0000	1.0000	1.000 000 000

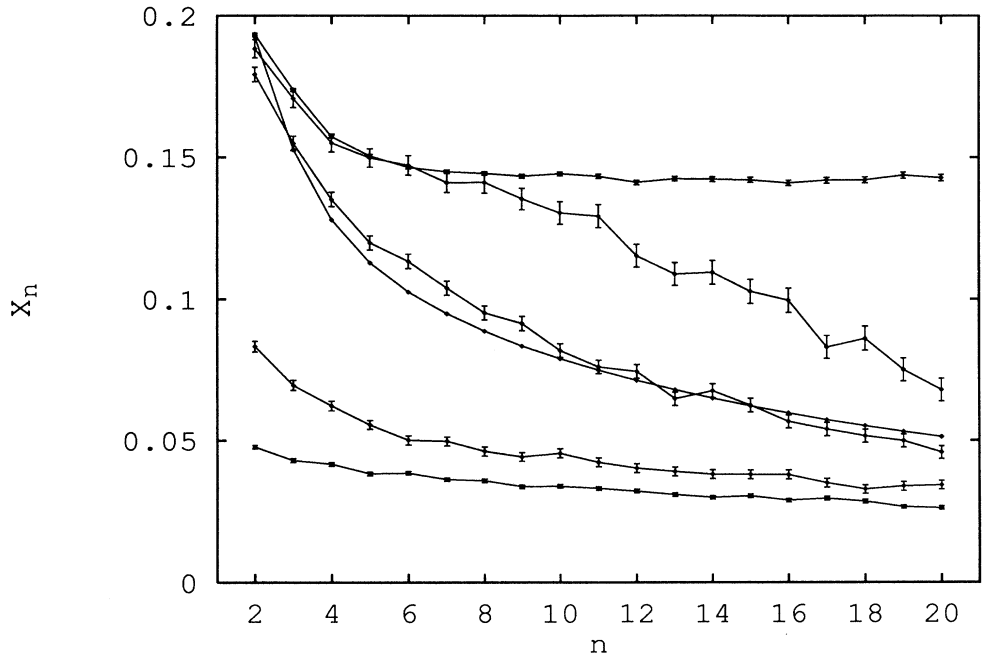

FIG. 6. X_n vs n for the RC model, with $C=1$, 0.998, 0.98, 0.8, and $\frac{2}{3}$ (top to bottom, curves with error bars). Also shown is the curve for the RC-BA model ($C=1$) (middle curve with no error bars). For $C<1$, no constant value is reached within the 2^{21}-step cutoff, indicating that the size distribution is not a power law. Lines connecting the data are to help guide the eye.

$C=0.98$ nearly follows that of the RC-BA model for $C=1$ (discussed in Sec. V), which is also plotted in this figure. The slow decrease in X_n for $C<1$ is suggestive of logarithmic behavior in $N(s)$.

An $N(s)$ containing logarithmic terms is known to occur for particles undergoing Markovian random walks on the lattice, which corresponds to the Boltzmann approximation in the RC model (RC-BA). In Sec. V, we show that for the RC-BA model, the asymptotic behavior of $N(s)$ is of the form

$$N(s)\sim\frac{a_3}{\ln s+c_3}\quad\text{or}\quad N_n\sim\frac{a_3}{n\ln 2+c_3} \tag{16}$$

for large s or n, where a_3 and c_3 are constants. On a plot of $1/N_n$ versus $n=\log_2 s$, the behavior represented by (16) will produce a straight line. In Figs. 7(a) and 7(b) we plot the data of the RC simulations for $C<1$ this way and find very good evidence for linearity for large n. As C decreases, the linear behavior extends to lower values of n. Figure 7(b) shows the data for $C=\frac{2}{3}$ on an enlarged scale, showing that linear behavior is followed to high precision. From the values of the slopes and intercepts, we have determined the values of a_3 and c_3, and these are listed in Table IV. Note that in Fig. 7(a) we also show the data for the RC-BA (for $C=1$), which falls very close to a straight line as predicted, and for contrast show the data for the simulations of the RC model when $C=1$. In the latter case, linear behavior is never reached, since $N(s)$ does not follow (16).

We consider in more detail the case $C=\frac{2}{3}$, which corresponds to the GSAT [35], and for which we have carried out the largest number of simulations (150 000) for the cases $C<1$. To make a sensitive test of the nature of the logarithmic behavior of $N(s)$, we consider that $N(s)$ follows the more general asymptotic form:

$$N(s)\sim\frac{a_3}{(\ln s+c_3)^m}\quad\text{for } s\to\infty\ , \tag{17}$$

where m is a constant, which implies that

$$X_n\sim\frac{m}{n\ln 2+c_3}\quad\text{for } n\to\infty\ . \tag{18}$$

If (17) is followed, then a plot of $1/X_n$ versus n will yield a straight line with slope $(\ln 2)/m$. In Fig. 8 we make this plot with the data for $C=\frac{2}{3}$. These data fall near a line with slope ln2 (implying $m=1$), thus providing further evidence that (16) is obeyed. The intercept of the line gives $c_3=23$, in agreement with the value found above (Table IV).

An interesting consequence of N_n obeying (16) is that the errors in X_n, calculated from (14), will be independent of n. Indeed, one can see in Fig. 6 that this is the case when $C<1$. Note that because X_n does not tend to a constant value, it is not useful to consider the quantity $\bar{X}_n$ here.

Thus, the RC model when $C<1$ acts like a random walk (the RC-BA model) with respect to the orbit-size

distribution (first-return probability). The straight segments where the path can cross evidently allow the particle to return to the origin after a given time with a probability that is appropriate for a simple random walk rather than a percolation cluster hull (for large times), no matter how low the concentration of those straight segments is. Yet, we will find (in Sec. IV B) that the properties of $\langle \Delta r^2(s) \rangle$ for the RC model ($C < 1$) are quite different from those of the RC-BA model.

B. Geometric properties

The geometric properties of the trajectories are characterized by the behavior of $\langle \Delta r^2 \rangle$, or its derivative func-

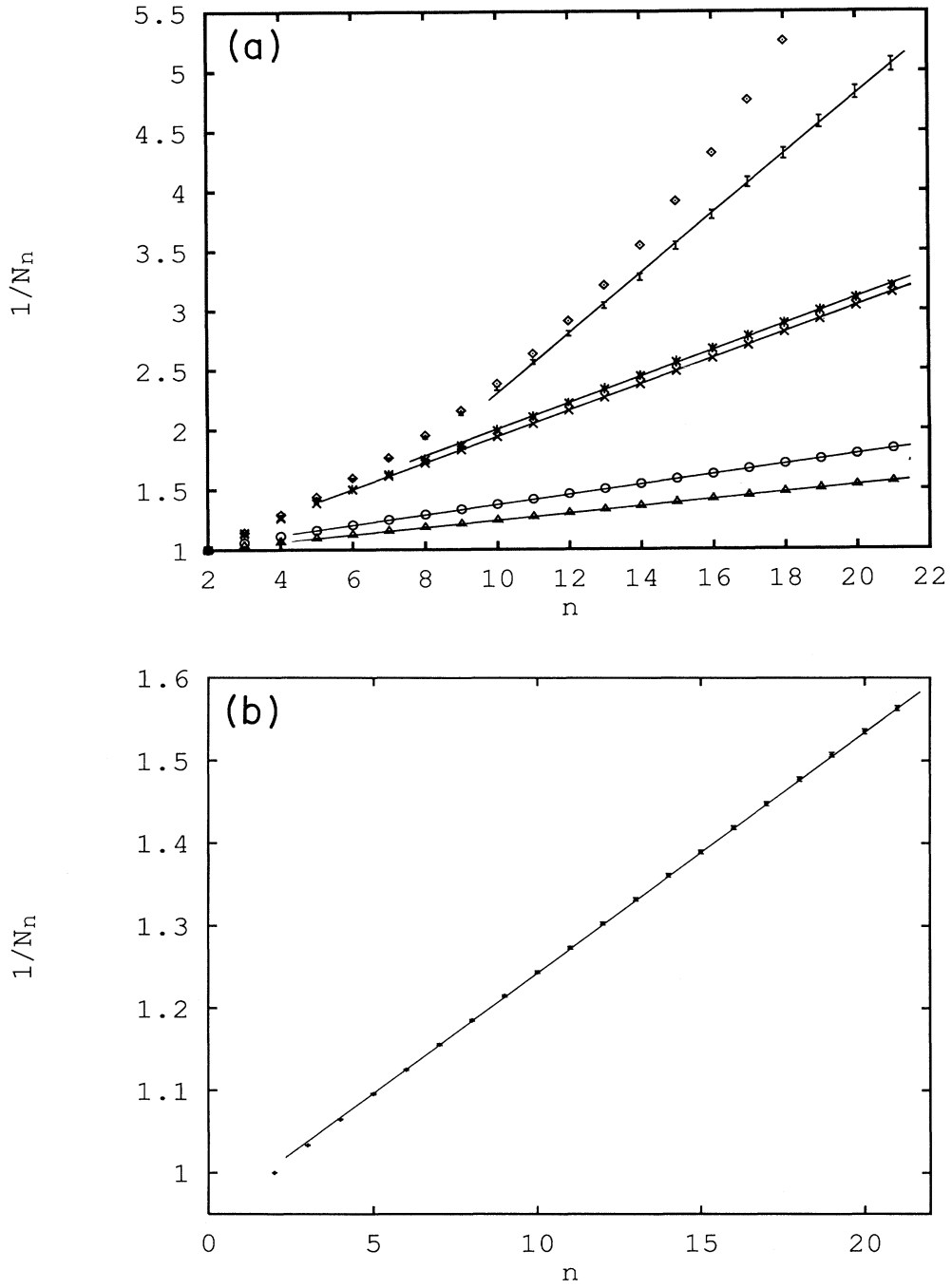

FIG. 7. (a) $1/N_n$ vs n for the RC model with $C=1$ ($\diamond$), 0.998 (error bars only), 0.98 ($*$), 0.8 ($\circ$), and $\frac{2}{3}$ ($\triangle$), and for the RC-BA model with $C=1$ ($\times$). In all cases besides 0.998, the error bars are smaller than the size of the symbols. (b) The curve for $C=\frac{2}{3}$ on a more expanded scale, clearly showing linear behavior.

TABLE IV. Values of a_3 and c_3 in (16), found by fitting a straight line to the data of $1/N_n$ versus n, for the RC model with $C<1$ and the RC-BA model with $C=1$. Also given is b_6 of (23), where $C_4=C_3$.

C	a_3	c_3	b_6
0.66	23.6	22.5	0.0037
0.8	16.3	15.5	0.0053
0.98	6.3	5.7	0.014
0.998	2.7	−8.2	
1.0 (BA)	6.28	5.28	

tion Y_n, defined in (11). Figure 9 shows the behavior of Y_n for the trajectories that reached the cutoff. For $C=0.998$ the deviations from the behavior of $C=1$ are small even at the longest distances measured, but for $C=0.98$, a drop-off can be seen already at $n\approx 11$. For $C=0.8$, Y_n does not follow the behavior for $C=1$ at any length scale. These curves appear to approach $Y_n=1$ as $n\rightarrow\infty$ in a slow (i.e., logarithmic) manner.

Again we look at the case of $C=\frac{2}{3}$ in more detail. We have replotted Y_n for this case in Fig. 10. The data for $s\leq 1000$ ($n\approx 11$) is close to Lyklema's results of the GSAT [35]. Lyklema believed that his data extrapolated (for an infinite system) to $2/d_f=1.070\pm 0.006$, which was close to the behavior of the last points he measured. However, our results do not bear out this prediction, since at $s=2^{16}$, Y_n is already below this value and is evidently still dropping.

Of course, one might wonder whether the general decrease we see in Y_n might be a consequence of the finite-size cutoff, considering that that cutoff was shown to cause Y_n to decrease (as n approaches n^*) for $C=1$. To investigate this point further, we carried out simulations at $C=\frac{2}{3}$ using an upper cutoff of 2^{24} steps. With this large value, the simulations are much more time consuming and we generated only 5000 trajectories, but because of their large size they yielded a sufficiently large number of distance measurements to obtain good (i.e., smooth) results for Y_n for $n\lesssim 18$. These data are also plotted in Fig. 10, and it can be seen that they are in close agreement with the data of $Y_n(n^*=21)$ for $n\lesssim 18$. The decrease in the $Y_n(n^*=21)$ at $n=19$ and 20 most likely reflects cutoff effects, while the erratic behavior of the $Y_n(n^*=24)$ when $n\geq 19$ is undoubtedly the consequence of there being an insufficient number of measurements. We conclude that the broad decrease in Y_n is not an effect of the finite cutoff. The deviation from the behavior predicted by Lyklema shows the importance of going to a large system in this study.

To get an idea of how $\langle \Delta r^2(s)\rangle$ might behave, we can relate it to the behavior of $N(s)$ by the following argument. In Ref. [18] it was shown that for all values of C, the ensemble-average mean-square displacement $\langle \Delta r^2(s)\rangle$ is proportional to the time, where the bar indicates an average over all starting points in the system. Here we explore the implications of this result. At a given time ($=s$), an individual particle of the ensemble

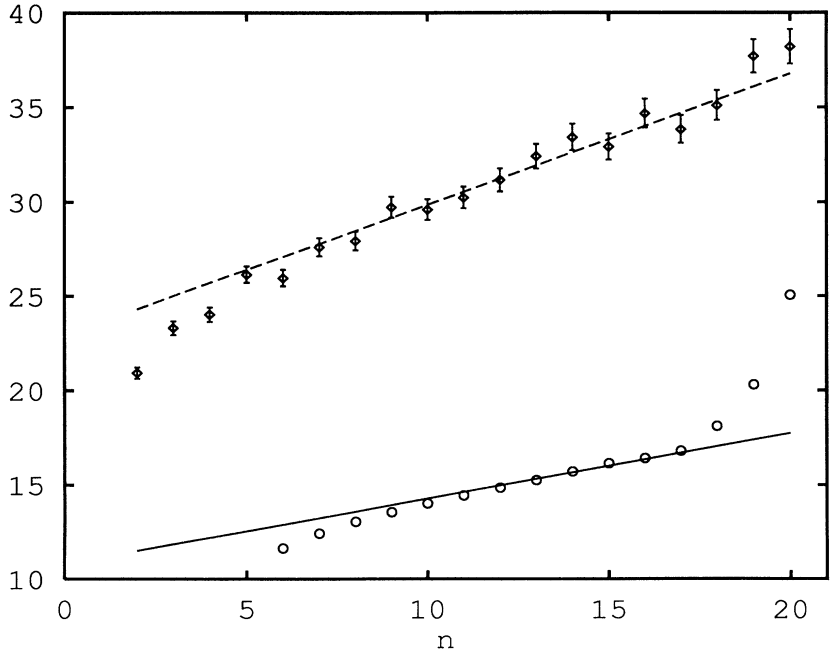

FIG. 8. Upper curve (◇), $1/X_n$ vs n for the RC model with $C=\frac{2}{3}$. A line of slope ln2 is drawn through the data, showing that they are consistent with (16), and the intercept implies $c_3\approx 23$. Lower curve (○), $1/(Y_n-1)$ vs n with a line of slope (ln2)/2 drawn through the data, showing that they are consistent with (23) with $p=2$. The intercept implies $c_4\approx 22$.

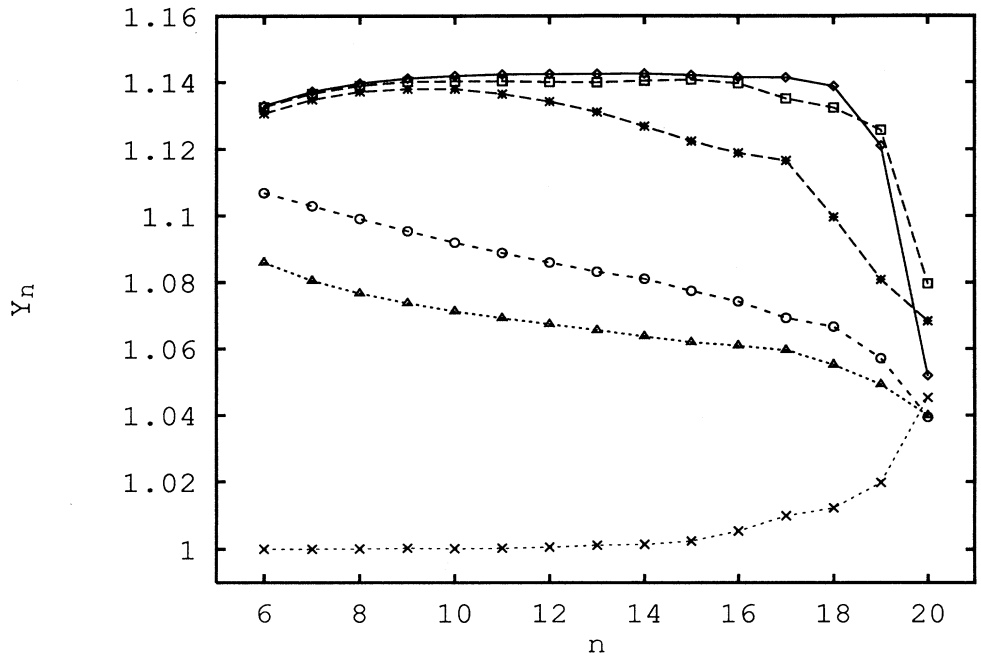

FIG. 9. Y_n for the RC model with $C=1$ (◇), 0.998 (□), 0.98 (∗) 0.8 (○), and $\frac{2}{3}$ (△). For $C<1$, no constant value is reached for large n, indicating that no consistent self-similar (fractal) behavior is attained. Also shown is the result for the RC-BA model with $C=1$ (×).

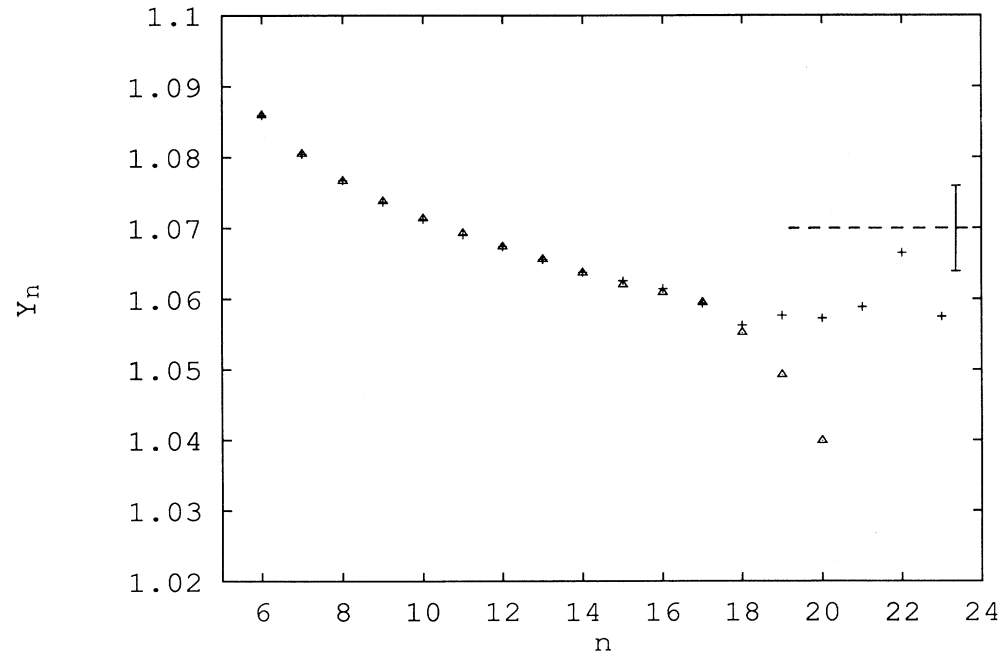

FIG. 10. Y_n for the RC model with $C=\frac{2}{3}$, which corresponds to the GSAT model [35]. Results are shown for cutoffs of 2^{21} (△) and 2^{24} (+) steps. These data are in general agreement with Lyklema's data, given for $s\leq 2000$ ($n\approx 11$), but they do not bear out his extrapolation to an infinite system (— — —, with error bar).

can either be moving on an open trajectory or in a closed orbit. As a consequence, we can write

$$\overline{\langle r^2(s)\rangle}=N(s)\langle r^2(s)\rangle_{\text{open }(s)}+\sum_{s'=1}^{s-1}P(s')\langle r^2(s)\rangle_{\text{closed }(s')}\ , \tag{19}$$

where $\langle r^2(s)\rangle_{\text{open }(s)}$ is the average mean-square distance between the first point (origin) and last point of open trajectories of s steps in length, while $\langle r^2(s)\rangle_{\text{closed }(s')}$ is the average mean-square distance between the origin and the point reached after s steps, on closed orbits of size s' steps, where $s>s'$. Here we use r^2 rather than Δr^2 to indicate that the distance is measured between the origin and the point s steps away, rather than between pairs of points along the path, as is done in determining $\langle \Delta r^2(s)\rangle$. The latter quantity is equivalent to $\langle r^2(s)\rangle_{\text{open }(s)}$ only when $s=s^*$. The quantity $\langle r^2(s)\rangle_{\text{closed }(s')}$ will be an oscillating function of s (for a fixed s'), since whenever s is an integer multiple of s' the particle will be back at the origin.

When $C=1$, the system is at a critical point, and one would expect that all measures of the mean-square distance will scale as in (2). Thus,

$$\langle r^2(s)\rangle_{\text{open }(s)}\sim b_2 s^{2/d_f} \quad \text{for } s\to\infty$$

$$\langle r^2(s)\rangle_{\text{closed }(s')}\sim b_3 (s')^{2/d_f} \quad \text{for } s>s' \text{ and } s'\to\infty \tag{20}$$

(where in the second case we describe the magnitude of the mean-square displacement since it is an oscillating function). Furthermore, for $C=1$, $P(s)$ follows (1) and $N(s)$ follows (7). Thus, (19) gives

$$\overline{\langle r^2(s)\rangle}\sim a_2 b_2 s^{2-\tau+2/d_f}+a_1 b_3 \sum_{s'\,(<s)} (s')^{1-\tau+2/d_f}$$

$$\sim (a_2 b_2+a_1 b_3)s \tag{21}$$

for large s, where we have made use of the hyperscaling relation $1-\tau=2/d_f$. Thus, one finds the average mean-square displacement is proportional to the time, as in ordinary diffusion [18]. It is interesting to look at the numerical values of the constants above. In Sec. III we found $a_1=0.162$ and $a_2=1.13$. We can find b_2 from the measurement of $\langle \Delta r^2(s)\rangle$ at $s=s^*$, since in that case it is equal to $\langle r^2(s)\rangle_{\text{open }(s)}$. Using the data for $s^*=2^{21}$ of Table II, we find $b_2=(2^{23.61}/2^{21})^{8/7}\approx 0.770$. Thus, the first term in (21) is $a_2 b_2\approx 0.87$. We cannot find the value of the second term (the contribution from closed orbits) because we have not determined the value of b_3 and the effect of the oscillations, but we expect it to be small. Indeed, the measurements [18] of $\overline{\langle r^2(s)\rangle}\sim 4Ds$ yield $4D\approx 0.89$, so we deduce that $a_1 b_3$ must be ≈ 0.02. Thus, the open trajectories contribute the most by far (0.87 versus 0.02) to $\overline{\langle r^2(s)\rangle}$.

For $C<1$, it is still found [18] that $\overline{\langle r^2(s)\rangle}\sim 4Ds$. If $N(s)$ behaves as in (16), then it follows from (19) that

$$\langle r^2(s)\rangle_{\text{open }(s)}\sim b_4 s(\ln s+c_3)\ ,$$
$$\langle r^2(s)\rangle_{\text{closed }(s')}\sim b_5 s(\ln s+c_3)^2\ , \tag{22}$$

where b_4 and b_5 are constants. Thus, these two measures of the mean-square displacement behave differently. Although we have not measured precisely these two functions, they suggest that the quantity that we did measure, $\langle \Delta r^2(s)\rangle$, is of a similar form:

$$\langle \Delta r^2(s)\rangle\sim b_6 s(\ln s+c_4)^p \tag{23}$$

for $s\ll s^*$, where p, b_6, and c_4 are constants. Equation (23) implies by (11) that

$$Y_n\sim 1+\frac{p}{n\ln 2+c_4} \tag{24}$$

for large n. If (23) is followed, a plot of $1/(Y_n-1)$ versus n will yield a straight line with slope $(\ln 2)/p$. In Fig. 8 we show this plot for data of $C=\frac{2}{3}$. The linear behavior of the plot supports the conjecture that $\langle \Delta r^2(s)\rangle$ obeys (23), and the value of the slope implies that $p\approx 2$. Furthermore, the intercept gives $c_4\approx 22$, so within errors we find $c_4=c_3$ [as (22) would suggest]. In the following, we will assume this equality holds. Analyzing the data for $\langle \Delta r^2\rangle$, we further find that $b_6\approx 0.0037$. In Table IV, we give the value of b_6 for $C=0.8$ and 0.98 also. For these cases, we also verified that $c_4\approx c_3$.

Note that while (16) applies to the RC-BA model, (19) does not. This is because in the BA the particles are never in closed orbits, but continue on different trajectories after returning to the origin. Thus, the mean-square distances in that case are not expected to follow the behavior of (22).

V. RESULTS FOR THE BOLTZMANN APPROXIMATION WITH $C=1$

A. Orbit-size distribution

In the Boltzmann approximation to the Ruijgrok-Cohen model, the encounters of the trajectory with the mirrors are treated as independent random processes, with no memory about the state of a site as to its occupation by a mirror when the site is revisited in the future. Here we consider $C_L=C_R=\frac{1}{2}$ (or $C=1$), in which case the particles are effectively undergoing a simple random walk which turns either right or left, with equal probability, at every step.

We can derive an exact recursive expression for the size distribution of closed trajectories, $P(s)$, for the RC-BA model. The closed trajectories are ones in which the particle first returns to the origin with a velocity in the original direction. These trajectories are analogous to the orbits considered in the RC model—but of course here the particle will not continue on the same trajectory after it leaves the origin for the second time, as it does in the RC model. Thus $P(s)$ is simply the first return probability for the random walk, which can be found using renewal theory [38]. We introduce $u(s)$ as the probability that a particle will return to the original state (position and direction of motion) after s steps, irrespective of how many times it has been there before. We label the steps in the four directions as R, L, U, and D for right, left, up, and down, respectively. If the initial velocity of the parti-

cle is in the direction R, then the final step must also be an R. For example, the two trajectories that can close in four steps are $(R)ULDR$ and $(R)DLUR$. Walks can only close in $4i$ steps, where i is an integer, and are made up of i steps in each of the four directions. The probability that a trajectory closes in $4i$ steps ($i \geq 1$) is given by

$$u(4i) = \begin{bmatrix} 2i \\ i \end{bmatrix}^2 \left[\frac{1}{2}\right]^{4i+1} \quad (i \geq 1) , \tag{25}$$

where $\binom{2i}{i}$ is the number of ways of choosing i L's and i R's out of a total of $2i$ L's and R's, and similarly for U's and D's, the factor $(\frac{1}{2})^{4i}$ represents the probability of making $4i$ given turns, and the additional factor of $\frac{1}{2}$ accounts for the requirement that the last step must be an R. Note that (25) is very similar to the corresponding expression for u for a standard random walk on a two-dimensional square lattice, where the walker can step in all four directions with equal probability—in which case the RHS of (25) gives $u(2i)/2$ [38].

According to the theory of recurrent events [38], $P(s)$ follows from $u(i)$ by

$$P(s) = u(s) - \sum_{i=1}^{s-1} u(i)P(s-i) \tag{26}$$

for $s \geq 1$. This relation allows $P(s)$ to be determined recursively. Using (26) we have evaluated $P(s)$ for $s \leq 2^{21}$, and then found the B_n using (3). While this calculation involved 2.5×10^{11} floating-point calculations (carried out on an IBM RS 6000 computer), we believe that the accumulated round-off errors were not significant. The results are shown in Table III. Evidently the B_n for the RC-BA model are smaller than those of the RC model (Table I). To illustrate why this is so, in Fig. 11 we show all trajectories that contribute to B_2 and B_3. Although there are many more possible trajectories that can close in 8 or 12 steps in the RC-BA model compared to the RC model (Fig. 3), they occur with lower probability, because a factor of $\frac{1}{2}$ must be associated with each turn of the trajectory. In contrast, in the RC model, a single mirror can be responsible for two turns, which leads to fewer factors of $\frac{1}{2}$ in the weights.

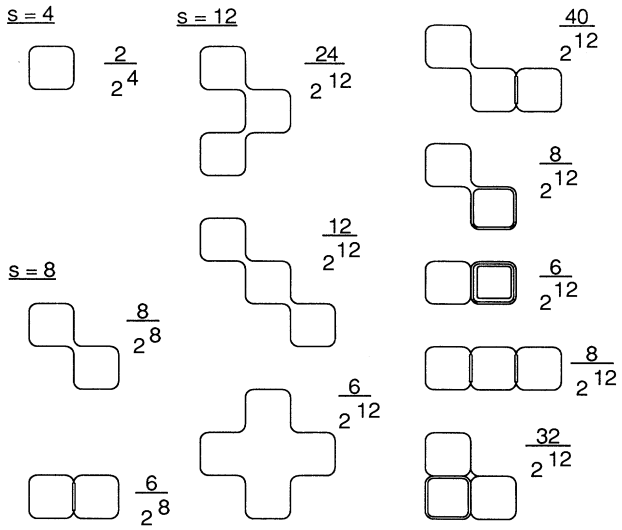

FIG. 11. Weights of first-return trajectories for the RC-BA model ($C=1$) for $s=4$, 8, and 12 steps. Double and triple lines indicate where a trajectory is traversed two or three times, respectively. In the bottom right diagram, there are two ways (clockwise and counterclockwise) to traverse the loop, giving an additional factor of 2 in the weight. The results for $s=4$ imply $B_2 = \frac{1}{8}$, and those for $s=8$ and 12 imply $B_3 = 14/2^8 + 136/2^{12} = \frac{45}{512} = 0.878\,906\,25$ in agreement with the values listed in Table III.

TABLE V. The mean-square distances $\langle \Delta r^2 \rangle$ and the resulting Y_n calculated from the 15 900 walks (out of 50 000 realizations) still open at the cutoff $s = 2^{21}$, for the RC-BA model ($C=1$).

n	$\log_2\langle \Delta r^2 \rangle$	Y_n
6	6.0002	1.0000
7	7.0001	1.0000
8	8.0001	1.0000
9	9.0001	1.0003
10	10.0005	1.0001
11	11.0006	1.0003
12	12.0009	1.0007
13	13.0016	1.0012
14	14.0027	1.0015
15	15.0042	1.0024
16	16.0067	1.0054
17	17.0120	1.0099
18	18.0219	1.0123
19	19.0342	1.0198
20	20.0540	1.0453
21	21.0993	

Equation (26) can be solved formally by generating function techniques. One finds that the generating function of $P(s)$ satisfies [38]

$$\bar{P}(z) \equiv \sum_{s=1}^{\infty} P(s) z^s = 1 - 1/\bar{U}(z) , \tag{27}$$

where

$$\begin{aligned} \bar{U}(z) &\equiv 1 + \sum_{i=1}^{\infty} z^{4i} u(4i) \\ &= \frac{1}{\pi} K(z^4) + \tfrac{1}{2} \\ &\sim -(1/2\pi)\ln(1-z) \quad \text{for } z \to 1 . \end{aligned} \tag{28}$$

Here $K(m)$ is the elliptic integral, as defined in Ref. [39]. By Tauberian theorems [38,40], (28) implies that

$$N(s) \sim \frac{2\pi}{\ln s + c_3} \tag{29}$$

and

$$P(s)=\frac{-dN(s)}{ds}\sim\frac{2\pi}{s(\ln s+c_3)^2} \tag{30}$$

for $s\to\infty$, where c_3 is a constant. Normally, the constant c_3 is not included in the expression for the asymptotic behavior for the return probability; we include it here as a way to conveniently take into account higher-order terms in $1/\ln s$. The $1/N_n$ that follow from (26) are plotted in Fig. 7, and the corresponding X_n are plotted in Fig.6. The slope of the line through the data in Fig. 7 is $\ln 2/2\pi$, consistent with (29), and the intercept gives $c_3=5.28$. Equation (29) was used in the analysis in Sec. IV, where it was found that $N(s)$ of the RC model for $C<1$ follows similar behavior.

B. Geometric properties

We also carried out simulations of the trajectories of the RC-BA model, to investigate their geometrical properties. Other than "forgetting" the state of the sites after visiting them, we carried out the simulation in much the same way as in Sec. III. We started with a particle at the origin, with an initial velocity in a given direction, and carried out a random walk that turned at each step. For those trajectories that never returned to the origin with a velocity in the initial direction when the cutoff $s^*=2^{21}$ was reached, we calculated $\langle\Delta r_n^2\rangle$ in the same way as in the RC model. From $\langle\Delta r_n^2\rangle$ we determined Y_n by (11). Of course, we did not need to put the mirrors on a lattice here as in the RC model simulations and instead used simple variables for the x and y coordinates of the position of the particle.

We carried out 50 000 trials in total. The size distribution of returning trajectories ("orbits") was binned as in the RC-model simulations; the resulting B_n were consistent with the exact values listed in Table III within error bars calculated from (13).

We calculated $\langle\Delta r^2\rangle$ and the resulting Y_n for all walks that reached the cutoff. For an unrestricted random walk, one would expect [18] that $\langle\Delta r^2\rangle\sim 4Ds$ with $D=\frac{1}{4}$ for large s, implying $Y_n\to 1$ for large n. However, because we consider only those walks that remain open when the cutoff is reached, discarding those that returned to the origin, we have biased the ensemble. As a consequence, $\langle\Delta r^2\rangle$ is not precisely proportional to s, and the Y_n are not precisely equal to 1. The values of Y_n are listed in Table V and are plotted in Fig. 9. It can be seen that $Y_n\approx 1$ for small separations, but as the cutoff is reached, the mean-square separation is somewhat larger than for a pure random walk, reflected in a small but significant increase in Y_n for the last few values in n.

These deviations of Y_n from unity are larger than the deviations we found in Y_n from the value $\frac{8}{7}$ for the RC model at $C=1$. For example, $Y_{15}-1=0.0026$ for the RC-BA model (Table V) while it is -0.0003 in the simulation of the RC model at $C=1$ (Table II). The deviations are positive in the RC-BA model, but negative in the RC model. In both cases, an open trajectory of 2^{21} steps has noticeably different properties than one would find on a piece 2^{21}-steps long of an infinite open trajectory. Thus, choosing specific trajectories to calculate mean-square displacement in random walks can cause subtle deviations in the expected behavior.

VI. CONCLUSIONS

We have studied the distribution of individual orbits and the geometric (fractal) properties of the trajectories for three distinct cases: (i) the RC model for $C=1$, which corresponds to hull percolation, (ii) the RC model for $C<1$, especially $C=\frac{2}{3}$, which corresponds to the GSAT with equal probability of stepping in any of the three allowed directions, and (iii) the RC-BA model for $C=1$. The three cases can be summarized in the following by comparing the behavior of $N(s)$ and $\langle\Delta r^2(s)\rangle$.

(i) For the RC model with $C=1$,

$$N(s)\sim a_2 s^{-1/7}, \tag{7'}$$

$$\langle\Delta r^2(s)\rangle\sim b_1 s^{8/7}; \tag{2'}$$

(ii) for the RC model with $C<1$,

$$N(s)\sim\frac{a_3}{\ln s+c_3}, \tag{16}$$

$$\langle\Delta r^2(s)\rangle\sim b_6 s(\ln s+c_3)^2; \tag{23'}$$

(iii) for the RC-BA model with $C=1$,

$$N(s)\sim\frac{2\pi}{\ln s+c_3}, \tag{29}$$

$$\langle\Delta r^2(s)\rangle\sim s \tag{31}$$

with $b_1=0.8315$, $a_2=1.13$, and $a_3(C)$, $c_3(C)$, and $b_6(C)$ given in Table IV.

For the RC model with $C=1$, we have verified the theoretical results for τ and d_f for percolation hulls to unprecedented accuracy. For the RC model with $C<1$, we found that the trajectories do not show simple fractal-like behavior, nor do the orbits follow a power-law size distribution for s as large as 2^{21}. The important difference between $C<1$ and $C=1$ is undoubtedly that in the former case the trajectory is allowed to cross itself. Allowing only 0.2% of the sites to have no mirrors ($C=0.998$) causes an easily noticeable change in the orbit-size distribution and in the behavior of the mean-square displacement. Evidently, a non-Brownian fractal ($d_f\neq 2$) is possible only for noncrossing trajectories, which occurs for $C=1$ only. When we allow the trajectories to cross, the mean-square displacement shows logarithmic behavior, implying that the trajectories are not self-similar. Our results support the conjecture of Bradley [23] that the GSAT, identical to the RC model for $C=\frac{2}{3}$, is not at a critical point. We have fit the data for $C<1$ to the logarithmic behavior of forms that were suggested by the RC-BA model. This logarithmic form implies that all trajectories will eventually close—there is a zero probability for the particle to escape to infinity (as a random walk in three dimensions does, for example [38]). We have not proven this result theoretically. For the RC-BA model with $C=1$, the results on the size distribu-

tion of "orbits" (recurrent circuits) were derived analytically. The orbit-size distribution in this case is qualitatively similar to the distribution found in the RC model for all $C<1$. We also carried out simulations to study the behavior of the mean-square distance.

We have made a general analysis of the statistical errors that would be expected from sampling a given distribution. This analysis makes it unnecessary to "batch" runs to determine the errors. This analysis does not apply to the measurement of $\langle \Delta r^2 \rangle$, but in this case one can determine the errors by keeping track of both $\langle \Delta r^2(s) \rangle$ and $\langle \Delta r^4(s) \rangle$ for all trajectories.

While we have answered many of the questions raised in the Introduction, this work suggests many more. We end with a list of some questions which we believe may be of interest for future investigation.

(1) For the cases of $C<1$, further simulations need to be carried out to investigate the nature of the orbits' size distribution and geometric properties. Especially, how do the various measures of the mean-square distance, $\langle \Delta r^2(s) \rangle$, $\langle r^2(s) \rangle_{\text{closed } (s')}$, and $\langle r^2(s) \rangle_{\text{open } (s)}$, behave? Do the latter two follow the behavior predicted in (22)? The apparent behavior of the size distribution (16) implies that all trajectories will eventually close. Can this be proven theoretically?

(2) For the geometric and fractal properties, we have considered only $\langle \Delta r^2 \rangle$. What is the behavior of the higher moments and of the distribution itself? This question is in analogy to that of the higher moments for the ensemble-averaged displacement, addressed in Ref. [18]. Can the system be described as a multifractal when $C=1$?

(3) How does the system behave when $C_L \neq C_R$? For $C_L + C_R = 1$, it is known [6] that the system is still at the percolation point, but the orbits become stretched out.

(4) For a large closed orbit when $C<1$, what is the behavior of the outside hull [41] (which is simply the boundary at the exterior of the orbit)? Is it a fractal with dimension $\frac{4}{3}$ as found by Grossman and Aharony [41] for percolation clusters ($C=1$) and by Mandelbrot [34] for Brownian trails (trails of a simple random walk)?

(5) Would the conclusions be generally the same for the Gunn-Ortuño (GO) model [8], where sites rotate rather than reflect particles? Note an interesting difference in reversibility between the two models: when a particle's velocity is reversed, the trajectory is retraced in the RC model, but not in the GO model.

ACKNOWLEDGMENTS

R.M.Z. thanks R. M. Bradley for useful discussions, and acknowledges support from the National Science Foundation Grant No. DMR 8619731. E.G.D.C. and X.P.K. acknowledge support from Grant No. DE-FG02-88 ER13857 of the Department of Energy.

APPENDIX: THE DIFFUSION COEFFICIENT IN THE BOLTZMANN APPROXIMATION

Here we derive the time dependence of the mean-square displacement of a particle from the origin $\langle r^2 \rangle$ for the RC-BA model. The second derivative of $\langle r^2 \rangle$ gives the velocity autocorrelation function (VACF), which has been determined by van Velzen and Ernst [21] for the RC model. The following derivation uses a somewhat different method than used in Ref. [21].

Following Ref. [18] (with some small changes in notation) we introduce $f_i(x,y,t)$ as the probability that a particle is going in the i direction at the lattice position (x,y) and at time t (here t replaces s in the text). These functions satisfy the following equations [18] (written in a shorthand notation):

$$\begin{aligned} f_0'(x+1,y) &= (1-C)f_0 + C_R f_1 + C_L f_3 , \\ f_1'(x,y+1) &= (1-C)f_1 + C_R f_0 + C_L f_2 , \\ f_2'(x-1,y) &= (1-C)f_2 + C_R f_3 + C_L f_1 , \\ f_3'(x,y-1) &= (1-C)f_3 + C_R f_2 + C_L f_0 , \end{aligned} \tag{A1}$$

where the dependence on t, as well as the dependence on x and y on the right-hand side [where every f is evaluated at (x,y)], has been suppressed. The prime on the left-hand side indicates that the function is evaluated at time $t+1$.

We are interested in finding out how the mean-square displacements $\langle x^2 \rangle$ and $\langle y^2 \rangle$ grow with time, for an initial condition of a single particle at the origin and equally likely to be going in any one of the four directions: $f_i(0,0,0)=\frac{1}{4}$ for $i=0,1,2,3$. To solve for the mean-square displacement, one essentially must diagonalize the above equations. This can effectively be carried out by inspection, as described below.

Consider the trajectory shown in Fig. 12. As explained in that figure, the particle's motion with respect to the coordinates $\xi = x+y$ is a simple one-dimensional walk in which the particle continues to jump in the same direction until a left mirror is struck, at which point the direction of the particle's motion is reversed. Reflecting off a right mirror does not change the sense of the motion in the ξ direction. Likewise, with respect to the coordinates $\zeta = x-y$, the direction of a particle's motion is unchanged until a right mirror is struck.

Thus, it is sufficient to consider only a one-dimensional walk that continues in the same direction with probability $1-c$ and changes direction with probability c at each lattice site, where $c=C_L$ for motion in the ξ direction and $c=C_R$ for motion in the ζ direction. Define $f_+(x,t)$ and $f_-(x,t)$ as the average number of particles going right and left, respectively, at position x and time t. These distribution functions satisfy the equations

$$\begin{aligned} f_+'(x+1) &= (1-c)f_+(x) + c f_-(x) , \\ f_-'(x-1) &= (1-c)f_-(x) + c f_+(x) , \end{aligned} \tag{A2}$$

where we have suppressed only the t variable and again the prime indicates time $t+1$. The initial condition is $f_+(0,0)=f_-(0,0)=\frac{1}{2}$, and $f_\pm(x,0)=0$ for all $x \neq 0$. We define the nth moments ($+$ and $-$) at time t by

$$\langle x^n \rangle_\pm \equiv \sum_{x=-\infty}^{\infty} x^n f_\pm(x,t) , \tag{A3}$$

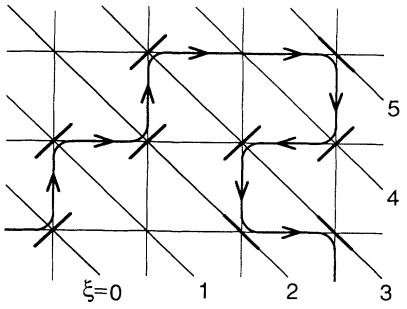

FIG. 12. A sample trajectory of a particle, used for the analysis of the RC-BA model. The values of constant $\xi=x+y$ are shown as diagonal lines. When the particle continues straight or reflects off a right mirror (probability $1-C_L$) the direction of the motion projected onto the ξ axis does not change, while when the particle reflects off a left mirror (probability C_L) the direction of the motion projected on this axis reverses. Thus, the motion of the particle projected on the ξ axis undergoes a one-dimensional random walk in which the probability of continuing in the same direction is $(1-C_L)$, and the probability of changing direction is C_L.

and introduce $\langle x^n\rangle\equiv\langle x^n\rangle_+ + \langle x^n\rangle_-$. For $n=0$, by summing (A2) over all x, we find

$$\begin{aligned}\langle 1\rangle'_+ &= (1-c)\langle 1\rangle_+ + c\langle 1\rangle_- ,\\ \langle 1\rangle'_- &= (1-c)\langle 1\rangle_- + c\langle 1\rangle_+ ,\end{aligned} \tag{A4}$$

which yields

$$\begin{aligned}\langle 1\rangle' &= \langle 1\rangle ,\\ \langle 1\rangle'_+ - \langle 1\rangle'_- &= (1-2c)(\langle 1\rangle_+ - \langle 1\rangle_-) .\end{aligned} \tag{A5}$$

The first equation in (A5) expresses the conservation of total probability, while the second shows how the difference in number between right- and left-moving particles changes when $c\neq\frac{1}{2}$.

For the first moment, we multiply the two equations in (A2) by $x+1$ and $x-1$, respectively, and sum over all x to find

$$\langle x\rangle'_+ = (1-c)[\langle x\rangle_+ + \langle 1\rangle_+] + c[\langle x\rangle_- + \langle 1\rangle_-] , \tag{A6}$$

$$\langle x\rangle'_- = (1-c)[\langle x\rangle_- - \langle 1\rangle_-] + c[\langle x\rangle_+ - \langle 1\rangle_+] .$$

Doing a similar calculation for the two second moments, and adding them together, we find

$$\langle x^2\rangle' = \langle x^2\rangle + 2(1-2c)[\langle x\rangle_+ - \langle x\rangle_-] + 1 . \tag{A7}$$

To solve this equation we need an explicit expression for the quantity $\delta(t)\equiv\langle x\rangle_+ - \langle x\rangle_-$. Taking the difference between the two equations in (A6), we find

$$\delta(t+1) = (1-2c)\delta(t) + 1 , \tag{A8}$$

which implies [since $\delta(0)=0$]

$$\begin{aligned}\delta(t) &= 1 + (1-2c) + \cdots + (1-2c)^{t-1}\\ &= [1-(1-2c)^t]/2c .\end{aligned} \tag{A9}$$

Next we write $\Delta(t)\equiv\langle x^2\rangle$. Equation (A7) becomes

$$\Delta(t+1) = \Delta(t) + 2(1-2c)\delta(t) + 1 . \tag{A10}$$

Using $\Delta(0)=0$, we find

$$\begin{aligned}\Delta(t) &= \sum_{n=0}^{t-1} [1 + 2(1-2c)\delta(n)]\\ &= t + \frac{(1-2c)}{2c^2}[2ct - 1 + (1-2c)^t] .\end{aligned} \tag{A11}$$

For long times, this implies $\Delta(t)\sim 2Dt$ with D given by

$$D = \frac{1-c}{2c} . \tag{A12}$$

In the limit that c is small and t is large, such that $ct=O(1)$, (A11) goes over to

$$\Delta(t) \sim \frac{1}{2c^2}(2ct - 1 + e^{-2ct}) , \tag{A13}$$

which is in the form of the Ornstein-Uhlenbeck expression for the mean-square displacement of a particle under the influence of a random force, in a one-dimensional continuum [37]. For times small compared to $1/c$, (A11) and (A13) are proportional to t^2, reflecting linear motion of the particle, while for long times it is proportional to t, reflecting diffusive motion. This model therefore represents an exactly soluble lattice representation of the Ornstein-Uhlenbeck process.

For the full two-dimensional problem, we have

$$\begin{aligned}\langle (x+y)^2\rangle &= t + \mathcal{L} ,\\ \langle (x-y)^2\rangle &= t + \mathcal{R} ,\end{aligned} \tag{A14}$$

where

$$\begin{aligned}\mathcal{L} &\equiv \frac{(1-2C_L)}{2C_L^2}[2C_L t - 1 + (1-2C_L)^t] ,\\ \mathcal{R} &\equiv \frac{(1-2C_R)}{2C_R^2}[2C_R t - 1 + (1-2C_R)^t] .\end{aligned} \tag{A15}$$

To get these expressions, we have simply replaced c in (A11) by C_L and C_R, respectively, as explained above. The second derivative of these expressions with respect to time gives the VACF as found by van Velzen and Ernst [21]. Taking the sum and difference of the two equations in (A14), we find

$$\begin{aligned}\langle x^2+y^2\rangle &= t + (\mathcal{L}+\mathcal{R})/2\\ \langle xy\rangle &= (\mathcal{L}-\mathcal{R})/4 .\end{aligned} \tag{A16}$$

By x-y symmetry, it follows that $\langle x^2\rangle = \langle y^2\rangle$, and for large t we find

$$\langle x^2\rangle \sim 2\left[\frac{C_L+C_R}{8C_L C_R} - \frac{1}{4}\right]t , \tag{A17}$$

where the term in parentheses is the diffusion coefficient for motion projected along the x axis, as given in Ref. [18]. When $C_L \neq C_R$, the diffusion is anisotropic and characterized by two different values [21] of D. These values can be found by examining the long-time behavior of the quantities in (A14), divided by 2, since the *unit* vectors in these directions are $(x+y)/\sqrt{2}$ and $(x-y)/\sqrt{2}$. In the direction of increasing $x+y$ (angle $\pi/4$), $D=(1-C_L)/4C_L$, while in the direction of increasing $x-y$ (angle $-\pi/4$), $D=(1-C_R)/4C_R$. These values of D are in agreement with the results of van Velzen and Ernst [21].

[1] T. W. Ruijgrok and E. G. D. Cohen, Phys. Lett. A **133**, 415 (1988).

[2] *P. Ehrenfest, Collected Scientific Papers,* edited by M. J. Klein (North-Holland, Amsterdam, 1959).

[3] E. H. Hauge and E. G. D. Cohen, Phys. Lett. **25A**, 78 (1967); J. Math. Phys. **10**, 397 (1969).

[4] G. Grimmett, *Percolation* (Springer-Verlag, Berlin, 1989).

[5] C. S. Smith, Leonardo **20**, 373 (1987).

[6] S. Roux, E. Guyon, and D. Sornette, J. Phys. A **21**, L475 (1988).

[7] B. Duplantier, J. Phys. A **21**, 3969 (1989).

[8] J. M. F. Gunn and M. Ortuño, J. Phys. A **18**, L1095 (1985).

[9] D. J. Gates, J. Math. Phys. **13**, 1315 (1972).

[10] R. M. Ziff, P. T. Cummings, and G. Stell, J. Phys. A **17**, 3009 (1984).

[11] P. Grassberger, J. Phys. A **19**, 2675 (1986).

[12] R. M. Bradley, Phys. Rev. A **39**, 3738 (1989).

[13] S. S. Manna and A. J. Guttmann, J. Phys. A **22**, 3113 (1989).

[14] P. G. de Gennes, La Recherche **7**, 919 (1976).

[15] H. E. Stanley, in *On Growth and Form,* edited by H. E. Stanley and N. Ostrowsky (Nijhoff, Dordrecht, 1986).

[16] D. W. Fisher, Z. Qiu, S. J. Shenker, and S. H. Shenker, Phys. Rev. A **31**, 3841 (1986).

[17] R. L. Blumberg-Selinger, S. Havlin, F. Leyvraz, M. Schwartz, and H. E. Stanley, Phys. Rev. **40**, 6755 (1989).

[18] X. P. Kong and E. G. D. Cohen, Phys. Rev. B **40**, 4838 (1989).

[19] X. P. Kong and E. G. D. Cohen, Physica D **47**, 9 (1991).

[20] X. P. Kong and E. G. D. Cohen, J. Stat. Phys. **62**, 1153 (1991).

[21] G. A. van Velzen and M. H. Ernst, J. Stat. Phys. **48**, 677 (1987); G. A. van Velzen, J. Phys. A **24**, 807 (1991).

[22] M. H. Ernst, G. A. van Velzen, and P. M. Binder, Phys. Rev. A **39**, 4327 (1989).

[23] R. M. Bradley, Phys. Rev. A **41**, 914 (1990).

[24] P. W. Kasteleyn, Physica **29**, 1329 (1963).

[25] A. Malakis, J. Phys. A **8**, 1885 (1975); **9**, 1283 (1976).

[26] A. Weinrib and S. A. Trugman, Phys. Rev. B **31**, 2993 (1985).

[27] K. Kremer and J. W. Lyklema, Phys. Rev. Lett. **54**, 267 (1985).

[28] R. Voss, J. Phys. A **17**, L373 (1984).

[29] B. Sapoval, M. Rosso, and J.-F. Gouyet, J. Phys. (Paris) **46**, L149 (1985).

[30] A. Bunde and J.-F. Gouyet, J. Phys. A **18**, L185 (1985).

[31] R. M. Ziff, Phys. Rev. Lett. **56**, 545 (1986).

[32] H. Saleur and B. Duplantier, Phys. Rev. Lett. **58**, 2325 (1987).

[33] R. M. Ziff, Physica D **38**, 377 (1989).

[34] B. B. Mandelbrot, *The Fractal Geometry of Nature* (Freeman, San Francisco, 1977).

[35] J. W. Lyklema, J. Phys. A **18**, L617 (1985).

[36] H. Meirovitch and H. A. Lim, Phys. Rev. A **38**, 1670 (1988); **39**, 4186 (1989).

[37] G. E. Uhlenbeck and L. S. Ornstein, Phys. Rev. **36**, 823 (1930).

[38] W. Feller, *An Introduction to Probability Theory and its Applications* (Wiley, New York, 1968), Vol. I, p. 359.

[39] *Handbook of Mathematical Functions,* edited by M. A. Abramowitz and I. A. Stegun (U.S. GPO, Washington, DC, 1965).

[40] E. W. Montroll and G. Weiss, J. Math. Phys. **6**, 178 (1965).

[41] T. Grossman and A. Aharony, J. Phys. A **19**, L745 (1987); **20**, L1193 (1987).